Nuclear Instruments and Methods in Physics Research A 810 (2016) 44–50

Contents lists available at ScienceDirect

Nuclear Instruments and Methods in Physics Research A

journal homepage: www.elsevier.com/locate/nima

Measurement of microwave radiation from electron beam in the atmosphere

I.S. Ohta [a], H. Akimune [a], M. Fukushima [b], D. Ikeda [b], Y. Inome [a], J.N. Matthews [c], S. Ogio [d], H. Sagawa [b], T. Sako [e], T. Shibata [f], T. Yamamoto [a,*]

[a] Faculty of Science and Engineering, Konan University, Kobe 658-8501, Japan
[b] Institute of Cosmic Ray Research, University of Tokyo, Kashiwa, Chiba 277-8582, Japan
[c] University of Utah, Salt Lake City, UT 4112-0830, USA
[d] Graduate School of Science, Osaka City University, Osaka 558-8585, Japan
[e] Solar-Terrestrial Environment Laboratory, Nagoya University, Nagoya 464-8601, Japan
[f] High Energy Accelerator Research Organization (KEK), Tsukuba 305-0801, Japan

ARTICLE INFO

Article history:
Received 10 November 2014
Received in revised form
14 November 2015
Accepted 15 November 2015
Available online 5 December 2015

Keywords:
Cosmic ray
UHECR
Microwave
Radio

ABSTRACT

We report the use of an electron light source (ELS) located at the Telescope Array Observatory in Utah, USA, to measure the isotropic microwave radiation from air showers. To simulate extensive air showers, the ELS emits an electron beam into the atmosphere and a parabola antenna system for the satellite communication is used to measure the microwave radiation from the electron beam. Based on this measurement, an upper limit on the intensity of a 12.5 GHz microwave radiation at 0.5 m from a 10^{18} eV air shower was estimated to be 3.96×10^{-16} W m^{-2} Hz^{-1} with a 95% confidence level.

1. Introduction

1.1. Observations of ultrahigh-energy cosmic rays

The origin of cosmic rays is one of the most intriguing enigmas in astronomy. In particular, cosmic rays with energy exceeding 5×10^{19} eV, called ultrahigh-energy cosmic rays (UHECRs), are considered to be created in extreme environments in extragalactic objects such as γ-ray bursts and active-galactic nuclei, although no experimental evidence has been found to support this theory. Huge observatories have been constructed to find the sources of UHECRs, such as the Pierre Auger Observatory [1,2] in the southern hemisphere and the Telescope Array (TA) Observatory [3,4] in the northern hemisphere. These observatories have confirmed UHECRs with energies exceeding 10^{20} eV with a rapid decrease in flux [5,6].

Recently, a hint of anisotropy was reported from the TA Observatory. An excess in the distribution of the arrival direction of cosmic rays above 57 EeV was reported. Nineteen events were detected within a 20° radius circle during five years of observations, whereas the expected value from an isotropic cosmic-ray sky is 4.49, the pre-trial significance of the excess is 5.1 sigma [7]. Furthermore, similar excess was reported in the southern sky from the Pierre Auger Observatory [8]. Increasing the statistics of the UHECR data is important to confirm these results. Furthermore, determining the mass of the primary UHECR is another key to revealing the acceleration mechanism. Therefore, next-generation UHECR detectors need to be sensitive to mass composition and have larger effective areas.

Detections of UHECRs are based on indirect measurements using particle detectors or atmospheric-fluorescence detectors (FDs) to measure extensive air showers. Particle detectors, called surface detectors (SDs), are spread over a wide area and measure the number of secondary particles from the air showers arriving on the ground. One advantage of SDs is that they provide continuous stable observation: however, they must be spread over a large area. Furthermore, SDs can only observe a single slice of an air shower. FDs use a remote-sensing technique to observe the isotropic radiation of ultraviolet photons emitted by air showers. This method allows us to observe the lateral distribution of secondary particles; however, it works only on clear and dark nights.

1.2. Detection of microwave radiation from extensive air showers

Similar to SDs, microwave radiation from air showers allows us to make uninterrupted observations of UHECR. Air showers radiate microwaves via geo-synchrotron radiation, which is caused by the geomagnetic field. The spectrum of Cherenkov radiation also spans

* Corresponding author.
E-mail address: tokonatu@konan-u.ac.jp (T. Yamamoto).

http://dx.doi.org/10.1016/j.nima.2015.11.113
0168-9002/

the microwave region. These processes cause polarized microwaves to be radiated in the forward direction along the shower axis. Apart from the radiation in the forward direction, isotropic microwave radiation may allow entire air showers to be remotely observed using the same approach as FDs. The small attenuation in the atmosphere is another advantage of observing air showers using isotropic microwave radiation. If the isotropic microwave radiation is sufficiently intense to be detected, next-generation techniques can be exploited to observe UHECRs, thereby allowing us to make measurements of the lateral shower development with an almost 100% duty cycle.

In this study, we describe a method to search the isotropic microwave radiation from an electron beam. In Section 2, we describe the detection principle. The experiment and the analysis of the results are presented in Section 3 Finally, the results are discussed in Section 4

2. Experiment

2.1. Molecular Bremsstrahlung radiation

An air shower comprises electromagnetic cascades, which create a huge number of secondary electrons and positrons. When the electron energy decreases to 84 MeV, which is the critical energy for electrons in the atmosphere, the air shower prevents further expansion of the cascades. At this stage, the number of secondary particles in the air shower is at its maximum, and Xmax denotes the atmospheric depth. The secondary electrons travel at the speed of light along the shower axis, creating a pancake-shaped shower front approximately 1 m thick. Beyond Xmax, the energy of the secondary electrons decreases from 84 to approximately 10 MeV at sea level. Therefore, the energy of most secondary electrons in an air shower ranges from 10 to 100 MeV.

The energy of the secondary electrons dissipate in the atmosphere through several processes. Part of the energy is converted into electromagnetic radiation through the Cherenkov and geo-synchrotron processes. Furthermore, the excitation of atmospheric molecules causes fluorescence emissions. A few tens of eV of the electron energy, in an atmospheric depth of 1 g/cm^2, are spent on this emission. However, approximately 2 MeV of the electron energy are deposited into this 1 g/cm^2 of atmosphere through ionization of the atmospheric molecules, which creates a plasma containing low-energy electrons with energies typically on the order of 1 eV. Because of their low energy, these electrons scatter in the atmosphere creating an isotropic plasma, which causes molecular Bremsstrahlung radiation (MBR) that radiates a spectrum up to the electron energy.

Previous studies experimentally confirmed MBR using electron accelerators [9]. They injected electron beams into an anechoic Faraday chamber and measured the intensity of the microwave emission in a perpendicular direction. In this study, at 0.5 m from a 3.36×10^{17} eV electron beam 0.65 m long, isotropic radiation was detected with an intensity of 4×10^{-16} $W/m^2/Hz$. Furthermore, the intensity of the radiation was proportional to the square of the beam energy. This result indicates that coherent radiation is emitted, which can be a great advantage for observing UHECRs. Coherent emission is caused when the emitting particles are distributed in a region smaller than the emission wavelength. If the emission is completely coherent, the intensity is proportional to the square of the number of electrons. Therefore, the intensity of the microwave emission depends on the density of the electrons. Based on the microwave emission intensity and its dependence on plasma density, instead of requiring detailed simulations, the microwave intensity from an air shower can be estimated using a simple scaling process.

However, one of the main problems in this experiment was noise from the accelerator and from the electron beam itself. Furthermore, the plasma density of the electron beam was lower than that of an actual air shower. Therefore, independent experiments that use extensive air showers are required to confirm these results.

Following this study, several experiments were performed to detect microwave emission from air showers in the gigahertz range. Some of them are listed below as follows:

- The CROME experiment has measured microwave signals at the KASKADE air-shower array in Germany to comprehensively study of the microwave radiation from air showers. This air-shower array can observe cosmic rays with energies below 10^{17} eV and detect forward radiation of gigahertz microwaves [10].
- AMBER, at the Pierre Auger Observatory, uses a 2.4-m-diameter parabola with sixteen receivers in the focal plane. The receivers are designed to detect C-band and Ku-band microwaves. The trigger signals for these measurements are provided by the Auger SDs [11,12].
- MIDAS, at the University of Chicago, USA, developed a 4.5-m-diameter telescope to detect MBR. Fifty-three C-band receivers are mounted in its focal plane. Despite constant observation with 61 days of live time, no candidate events were detected. Based on this result, an upper limit on the intensity of MBR from a 10^{17} eV air shower at 0.5 m from its Xmax was estimated to be 2.3×10^{-16} – 4.6×10^{-15} $Wm^{-2}Hz^{-1}$ with a 95% confidence level, depending on the coherent spatial properties of the plasma. This telescope has been relocated to the Pierre Auger Observatory [11–13].
- EASIER uses gigahertz receivers that are mounted on the SDs in the Pierre Auger Observatory directly, without using a parabola. The receivers are directed toward the zenith so that forward radiation from air showers can be observed using secondary particles. The first clear air shower microwave event was detected by this experiment in June 2011 [11,12].

2.2. Microwave detectors

An accelerationfs electron beam can be accurately controlled, unlike an actual air shower. However, the detectors need to be in an anechoic chamber near the accelerator, and therefore, the detection is limited by various sources of noise. Motivated by these experiments, we emitted electron beams into the atmosphere and measured the 12.5 GHz isotropic microwave radiation using a parabolic antenna. The observation system uses satellite communication devices as indicated in Fig. 1. The system uses an off-axis parabola (Nippon Antenna CS-S120K) with 1.32 and 1.22 m diameters in the major and minor axes, respectively. The radiation angle of 22.64° imposes a 1.17 m^2 aperture, which is equivalent to a 1.2-m-diameter circular reflector. The catalog for this antenna lists an antenna gain of 42.1 dBi at 12.5 GHz. The effective aperture A_R at the wavelength $\lambda = 0.0240$ m (12.5 GHz), can be estimated as follows:

$$A_R = \frac{0.0240^2}{4\pi} 10^{\frac{42.1}{10}} = 0.742 \text{ m}^2 \quad (1)$$

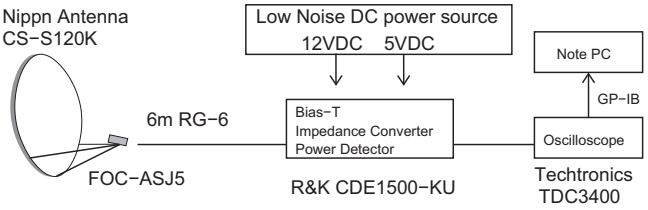

Fig. 1. Schematic of the observation system.

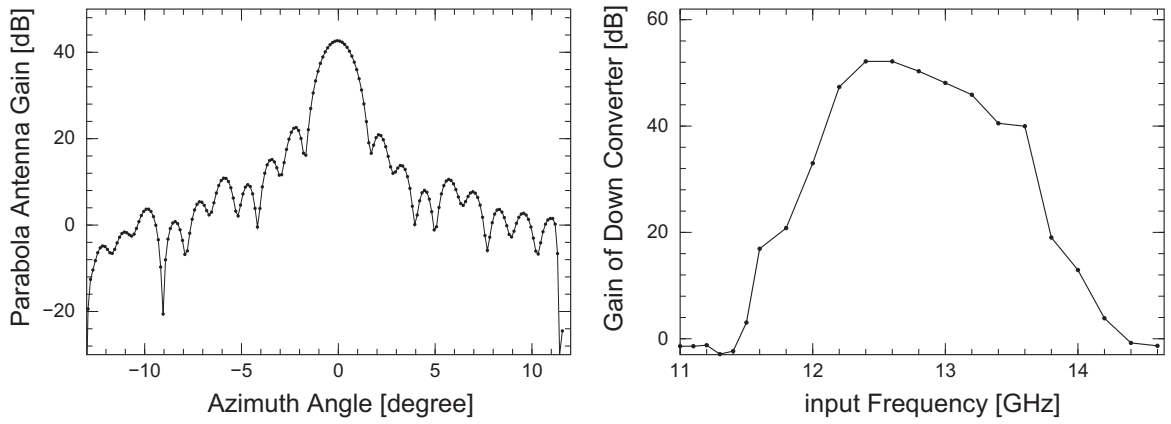

Fig. 2. Results of the calibrations of the microwave receiver. The gain and beam pattern of the parabola with the feedhorn is shown in the left panel. The peak value of the antenna gain is 42.7 dB. The gain of the down converter as a function of the frequency of the input microwave is shown in the right panel. The gain at 12.5 GHz is 52.2 dB. The results of these measurements are consistent with the values in the catalog, although the bandwidth of the down converter is slightly wider. These measurements were performed at the Microwave Energy Transmission Laboratory at Kyoto University [14].

Table 1
Devices for treating RF signals. The gains and attenuations of the devices are quoted from specifications provided by the manufacturers. These values are calibrated in the laboratory as explained in the text. The total gain from the parabola to the power detector is 118 dB.

	Product	Gain
1.2-m-diameter parabola	Nippon antenna CS-S120K	42.1 dBi
Feedhorn and down converter	Nippon antenna FOC-ASJ5	54 ± 6 dB
Booster (amplifier)	Nippon antenna CSB-C25-SP	23 ± 2 dB
6 m 75 Ω coaxial cable	RG-6	−1.4 dB/6 m
Bias-T, impedance converter, power detector	R&K CDE1500-KU	
1 m 50 Ω coaxial cable	RG-174/U	

Therefore, the antenna efficiency is

$$\frac{A_R}{1.17\ \mathrm{m}^2} = 0.657 \tag{2}$$

A feedhorn receiver with bandwidth of 12.25–12.75 GHz (Nippon Antenna FOC-ASJ5) is mounted at the focal point. The receiver uses two channels to measure the vertical and horizontal polarizations. The microwave signal is down converted to 0.95 – 1.45 GHz using a local oscillator with a frequency of 11.3 GHz. This down converter amplifies the signal by 54 ± 6 dB.

To verify the abovementioned catalog values, the sensitivity of the parabolic antenna was measured in the anechoic room of the Microwave Energy Transmission Laboratory at Kyoto University [14]. A 12.5 GHz microwave signal was transferred into the feedhorn from a network analyzer and reflected at the antenna. A two-dimensional radio scanner measured the near field to estimate the antenna pattern and the gain. The estimated antenna gain is 42.7 dB, which is consistent with the catalog value (Fig. 2). The field of view of the parabola was expected to be $1.22 \times \lambda/1.2\ \mathrm{m} = 1.40\ ^\circ$, which is also consistent with the results shown in Fig. 2. The bandwidth and gain of the down converter were also measured (Fig. 2). As can be seen in the figure, the bandwidth is slightly greater than 0.5 GHz.

The radio frequency (RF) signal from each channel passes through an amplifier (Nippon Antenna CSB-C25-SP), which amplifies input signal with a gain of 20 – 25 dB.

After the amplifier, the RF signal is transferred to an electronic device through a 75 Ω impedance, 6-m-long RG-6 cable with an attenuation factor of −1.4 dB. Therefore, the total gain from the parabola to the electronic devices through the coaxial cable is 118 ± 8 dB based on the specifications of the devices, as shown in Table 1. The electronic device for this project was developed with the R&K Company. Packed into a $3 \times 6 \times 2\ \mathrm{cm}^3$ (Fig. 3) aluminum box, this device (R& K-CDE1500-KU) provides the following three functions:

Fig. 3. Electric-circuit unit R&K CDE1500-KU developed with the R&K Company. A bias-T, impedance converter, and power detector are packed into a compact case.

- Bias-T: This provides a 15 VDC bias to the receiver and amplifier. The RF signal from the receiver goes through this circuit.
- Impedance converter: The RF signal is transferred through a coaxial cable with 75 Ω impedance to reduce the attenuation in the cable. The impedance is converted to 50 Ω to match the subsequent devices.
- Power detector: The amplitude of the RF signal is converted to DC voltage. A logarithmic detector (R& K AD8318) that uses an amplifier (MAX4003) to measure the power level of the RF signal up to 2.5 GHz with a response time of 11 ns is integrated into this part of the circuit. The dynamic range of this detector ranges from −60 to −10 dB m.

The output signal from CDE1500-KU is transferred through a coaxial cable to an oscilloscope (Tektronics TDC3400) and digitized when triggered by a signal from the ELS. Next, the digitized data is sent through GPIB to a notebook computer, which records the data on a hard disk.

The RF signal detected by the receiver is transferred to the oscilloscope through the detector chain, which is calibrated using a signal generator. The sinusoidal signals from the signal generator

go through the entire detector chain from the amplifier to the oscilloscope. Calibrating this chain includes the amplification and attenuation due to the cable, amplifier, and electronic devices. Therefore, we measured the function to convert the signal intensity from the down converter to a DC voltage measured by the oscilloscope. The result of this calibration is shown in Fig. 4. Based on this result, the conversion function was estimated as follows:

$$V\ \mathrm{mV} = -1.08(\pm 0.04) \times P\ \mathrm{dBm} + 13.4(\pm 1.42) \quad (3)$$

As shown in Fig. 4, this conversion function works well in the range from 0.95 to 1.45 GHz. The gains and the conversion factors of the two channels agree within the statistical errors of the measurements.

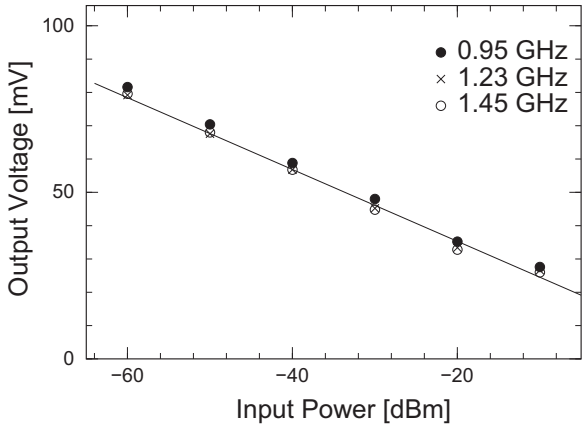

Fig. 4. Power detector DC output voltage as measured by the oscilloscope and as a function of the intensity of the amplifier input signal.

2.3. Electron emitter

The ELS was constructed at the TA observatory in Utah, USA, to calibrate the FDs that detect the ultraviolet photons from air showers (Fig. 5) [15]. The ELS can emit up to 10^9 electrons with an energy of 40 MeV as a pulse beam of width ranging from 20 ns to 1 μs. For our measurements, the total pulse charge of the beam was adjusted to 100 pC. Therefore, the beam contained 6.3×10^8 electrons. The energy deposited in the atmosphere by the 40 MeV

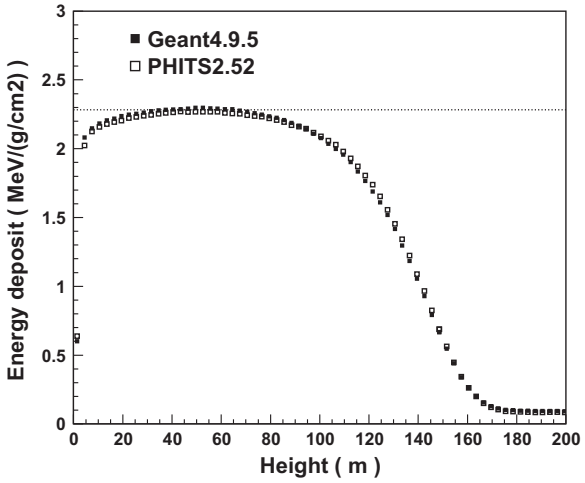

Fig. 6. Results of simulations using GEANT v4.9 [17] and PHITS v2.52 [18]. Energy deposited in the atmosphere by a 40 MeV electron from the ELS as a function of height above the ground. The energy deposited is primarily dissipated by ionization of atmospheric molecules.

Fig. 5. Photographs of the observation system installed at the TA observatory. The upper panel shows the parabola located in front of the FD building. The lower-left panel shows the parabola as seen from behind. The ELS is visible 85 m away from the parabola. The lower-right panel shows the data-acquisition system. The entire system is packed into a suitcase that can be transferred by commercial air flight from the laboratory to the observation site.

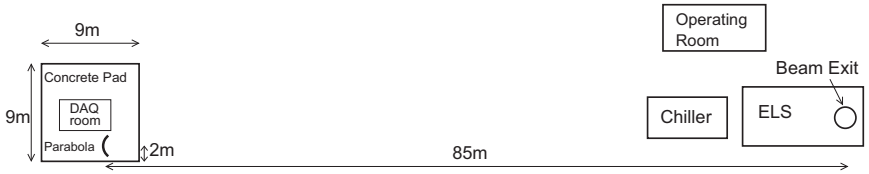

Fig. 7. Schematic of the arrangement of the ELS and the parabola. The parabola is located on a concrete pad 85 m from the ELS. The elevation angle of the parabola is 15°.

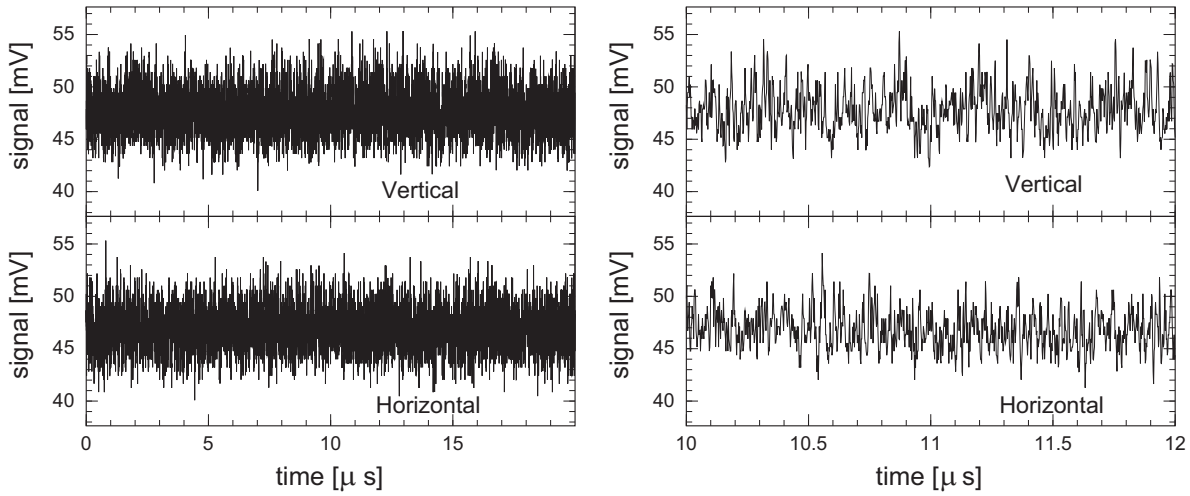

Fig. 8. Typical output-signal waveform from the power detector, as measured by the oscilloscope. Vertically and horizontally polarized signals were measured. The left panels show a 20 μs long waveform and the right panels show the same signal but from 10 to 12 μs. A negative pulse from 11.31 to 11.34 μs was expected. No clear pulse was observed.

electrons as a function of height above the ground was estimated using Monte Carlo simulations, as shown in Fig. 6. At 20 m above ground level, 2.3 MeV/(g/cm^2) is deposited by one 40 MeV electron. Therefore, the total energy deposited by the electron beam at 20 m is 1.4×10^{15} eV/(g/cm^2). This value is equivalent to the energy deposited by an air shower with an energy of 1×10^{18} eV at Xmax [16]. The fluorescence emission from this beam is too intense to be observed by the FDs. To avoid possible damage to the FD cameras, this observation was made during the day, when the FDs were not operating. The pulse shape of the beam was a triangle with a base width of 20 ns. Therefore, 87.5% of the electrons were contained in 10 ns. However, the plasma density of the beam was lower than that of an actual air shower, where plasma decays in 5 ns according to measurements [9].

3. Observation and analysis

The observation was made in May, 2013. The parabola was fixed on a concrete pad that was constructed to accommodate the various uses of the ELS (Fig. 7). Using a laser beam, the azimuthal direction of the parabolic antenna was adjusted toward the beam exit of the ELS with an accuracy of 0.1°. The elevation angle was 15° and the parabolic antenna was 88.0 m from the electron beam, as measured in the field of view of the antenna. Because the field of view of the antenna at 12.5 GHz is 1.40°, the beam length in the field of view was 2.23 > m.

A typical example of an event recorded by the oscilloscope is shown in Fig. 8. The signal is digitized with 2 ns sampling for 20 μs around a trigger pulse. The trigger pulse comes from the ELS and arrives at 4 μs (Fig. 8). The electron beam was emitted 7.80 μs after the trigger pulse and the cable delay of the trigger pulse was 0.75μs. Furthermore, the 88.0 m distance from the electron beam to the parabolic antenna resulted in an additional delay of 0.26 μs. Altogether, the MBR signal in Fig. 8 is expected to begin at $4+7.05+0.26=11.3$ μs. It took 7.4 ns for the electron beam to pass the field of view. The decay time of the low-energy electron plasma was 5 ns according to [9]. Moreover, the full width of the beam was 20 ns. Consequently, a negative 32.4 ns wide pulse was expected in both the horizontal and vertical polarizations starting at 11.31 μs. The response time of the power detector (11 ns) acts to widen the signal waveform. We have not included the time response of the power detector in our analysis.

To increase the signal sensitivity, we estimated the average waveforms for the 1797 events measured in this observation. As explained above, the expected pulse width of the signal was 32.4 ns, without accounting for the power detector response, which corresponds to 15.2 samples of the digitized signal. In the analysis, ten samples were integrated to estimate the waveform over a 20 ns time window. The result of this analysis is shown in Fig. 9. A microwave signal from the ELS beam would appear as a negative pulse at 11.32 μs. However, no signal can be seen in Fig. 9. Based on this result, we estimate an upper limit for the intensity of the microwave radiation as follows.

The signals from the horizontal and vertical polarizations differ slightly. For this estimate, the smaller value was used to generate a conservative result, i.e., the vertical polarization, which is 47.577 $\pm$ 0.027 mV as indicated in Fig. 9. The error indicates a 1 σ fluctuation. Therefore, the upper limit at a 95% confidence level is $47.577+0.027 \times 1.96=47.524$ mV.

This value can be converted from the output voltage of the power detector to the input power of the booster using Eq. (3). The power obtained is -31.60 ± 0.59 dB m. The error corresponds to a 1σ systematic uncertainty in the calibration. The input power of the 12.5 GHz microwave to the down converter was then estimated. The gain of the down converter was measured as indicated in Fig. 2, i.e., 52.2 dB. In this analysis we use 54 dB from Table 1 to generate a conservative result. With the adding of -54 dB, this

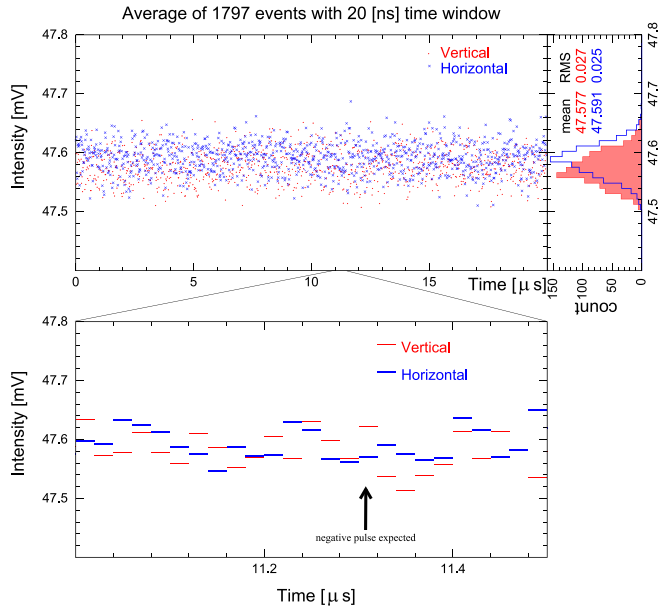

Fig. 9. Average waveform of the integrated intensity in a 20 ns time window over 1797 events. Signals from ten neighboring samples were integrated for each 2 ns sample. Positive 32.4 ns wide pulses starting at 11.31 μs were expected. No signal can be seen in this measurement.

Table 2
Comparison of present work with that of Ref. [9].

	Gorham et al.	Present work
Observed reference shower length	0.65 m	2.23 m
Reference shower equivalent energy	3.36×10^{17} eV	10^{18} eV
Observed center frequency	3.80 GHz	12.5 GHz
Distance to shower axis	0.5 m	0.5 m
Flux density $\mathrm{Wm^{-2}Hz^{-1}}$	4.00×10^{-16}	$< 3.97 \times 10^{-16}$

value changes to -85.60 ± 0.59 dBm $= (2.756 \pm 0.374) \times 10^{-9}$ mW.

Dividing this value by the effective aperture A_R, the upper limit of the microwave intensity at the parabolic antenna can be estimated. A_R for the far field is given by Eq. (1). However, the distance of 88 m cannot be approximated as far field because the Fraunhofer distance is $2 \times 1.2^2/\lambda = 120$ m. The distance of 88 m can only be considered as far field if the diameter of the parabolic antenna is less than 1.03 m. Therefore, we use this value to estimate the upper limit as follows:

$$I_{para} = \frac{\left(2.76 \times 10^{-9} \pm 0.37\right) \times 10^{-9}\ \mathrm{mW}}{0.742\ \mathrm{m^2} \times \frac{1.03^2}{1.2^2} \times 500 \times 10^6\ \mathrm{Hz}} = (10.09 \pm 1.37) \times 10^{-21}\ \mathrm{Wm^{-2}Hz^{-1}} \quad (4)$$

Then, the upper limit is as follows:

$$10.08 + 1.37 \times 1.96 = 12.77 \times 10^{-21}\ \mathrm{Wm^{-2}Hz^{-1}} \quad (5)$$

This value constitutes an upper limit on the microwave intensity 88 m from the electron beam with a confidence level of 95%. Therefore, the upper limit at 0.5 m from the beam can be estimated by a simple scaling as follows:

$$12.77 \times 10^{-21}\ \mathrm{Wm^{-2}Hz^{-1}} \times \frac{88^2}{0.5^2} = 3.96 \times 10^{-16}\ \mathrm{Wm^{-2}Hz^{-1}} \quad (6)$$

In summary, the cable delay and response time of the detectors have been measured and included in the analysis. The response time of the power detector (11 ns) was ignored. We have checked the influence of the length of the input signal waveform on the power detector. A 10-ns-short-microwave pulse and a long-sinusoidal signal have been injected into the booster and the output voltages from the power detector have been compared. We did not find a significant effect from the length of the input signal on this measurement. The gains of the parabola and the down converter were measured as shown in Fig. 2. However, in this analysis, these values were quoted from the specifications of these devices (Table 1) to generate a conservative result. The errors of these values were ignored.

4. Conclusion

We studied the isotropic microwave radiation from air showers using an ELS. This radiation source was proposed for UHECR research in [9], which reports detection of the MBR using electron accelerators. To confirm the existence of this radiation, we attempted to detect 12.5 GHz isotropic microwave radiation from electron beams using a 1.2 m diameter parabolic antenna. An ELS was used to generate a 20 ns wide pulsed beams of 40 MeV electrons. Each pulse contained 6.3×10^8 electrons and a total charge of 100 pC. The energy deposited in the atmosphere by this electron beam was equivalent to that deposited near Xmax by an air shower with an energy of approximately 10^{18} eV. The parabolic antenna was positioned 88 m from the electron beam. No significant signal was detected. This null result places an upper limit on the intensity of the isotropic emission of 12 GHz radio waves from an air shower with an energy equivalent to 10^{18} eV at 0.5 m from the shower axis. This limit is estimated to be 3.97×10^{-16} $\mathrm{Wm^{-2}Hz^{-1}}$ with a 95 % confidence level. This upper limit is close to that found in [9], but the two results cannot be compared directly because the experiments were configured differently (e.g., the detector bandwidths and the reference beam lengths differed). The differences between the two measurements are listed in Table 2.

Measurements of radio emissions using an electron accelerator are hindered by various sources of noise, including Cherenkov radiation from the electron beam and the electric noise from the electron accelerator. In the present study, the noise was largely suppressed by separating the detectors from the accelerator. We confirmed that the electric noise from the ELS was negligible at the separation distance. The noise level did not vary irrespective of whether the ELS was on or off. Furthermore, we located a microwave source in the path of the electron beam and confirmed that it was detected adequately. When the feedhorn with the data acquisition system was located close to ELS, the noise from the electron accelerator could be clearly seen depending on the stage of the acceleration.

This experiment is being upgraded to improve its sensitivity to MBR. In particular, the following improvements are being considered for the next measurements:

- reducing noise, particularly the thermal noise in the receiver and the down converter,
- moving the parabola closer to the electron beam, and
- increasing the intensity of the electron beam.

Acknowledgements

The authors thank the Telescope Array collaboration for their assistance, and the CROME and MIDAS collaborations, particularly Proffessor Ralph Engel, Dr. Radomir Smida, Proffessor Paolo Privitera, and Dr. Pedro Facal for useful discussions and suggestions. The detectors were calibrated using the facilities at the Microwave Energy Transmission Laboratory, Research Institute for Sustainable

Humanosphere. This work is supported by the Ministry of Education, Culture, Sports, Science and Technology, Japan, by a Grant-in-Aid for Scientific Research (B), 24340059, 2012 and a Grant-in-Aid for Challenging Exploratory Research, 21654036, 2009. Furthermore, it is partly supported by the Inter-University Research Program of the Institute of Cosmic Ray Research, University of Tokyo. The authors would like to thank Enago (http:www.enago.jp) for the English language review.

References

[1] J. Abraham et al. (The Pieere Auger Collaboration), Nuclear Instruments and Methods A 523 (2004) 50.
[2] ⟨http://www.auger.org⟩.
[3] T. Abu-Zayyad, et al., Nuclear Instruments and Methods A 689 (2012) 87.
[4] ⟨http://www.telescopearray.org⟩.
[5] J. Abraham, et al., Physics Letters B 685 (2010) 239.
[6] R.U. Abbasi, et al., Physics Letters B 100 (2008) 101101.
[7] The Telescope Array Collaboration, Astrophysics Journal 790 (2014) 21. http://dx.doi.org/10.1088/2041-8205/790/2/L21.
[8] The Pieere Auger Collaboration, Astrophysics Journal 804 (2015) 15. http://dx.doi.org/10.1088/0004-637X/804/1/15.
[9] P.W. Gorham, et al., Physics Review D 78 (2008) 032007.
[10] R. Smida, F. Werner, R. Englel, et al., Physics Review Letter 113 (2014) 221101.
[11] P. Allison for The Pierre Auger Collaboration, Proceedings of the 32nd International Cosmic Ray Conference (Beijing), 2011.
[12] R. Gaïor for The Pierre Auger Collaboration, Proceedings of the 33rd International Cosmic Ray Conference (Rio de Janeiro), 2013.
[13] J. Alvarez-Muñiz, et al., Physics review D 86 (2012) 051104 , R.
[14] ⟨http://www.rish.kyoto-u.ac.jp/English/METLAB/index.html⟩.
[15] T. Shibata, et al., Nuclear Instruments and Methods A 597 (2008) 61–66.
[16] M. Unger, et al., Nuclear Instruments and Methods A 588 (2008) 433.
[17] GEANT, CEAN Program Library Long Writeup W5013. ⟨http://www.asd.web.cern/wwwasd/⟩.
[18] K. Niita, et al., Radiation Measurement 41 (2006) 1080–1090.